
CHEMICALLY AWARE UNITARY COUPLED CLUSTER WITH *AB INITIO* CALCULATIONS ON SYSTEM MODEL H1: A REFRIGERANT CHEMICALS' APPLICATION

OCTOBER 27, 2022

I. T. Khan, M. Tudorovskaya, J. J. M. Kirsopp, D. Muñoz Ramo
Quantinuum, Terrington House, 13–15 Hills Road, Cambridge CB2 1NL, United Kingdom

P. Warrier, D. K. Papanastasiou, R. Singh
Honeywell Advanced Materials, 20 Peabody St, Buffalo, NY 14210, United States

Abstract

Circuit depth reduction is of critical importance for quantum chemistry simulations on current and near term quantum computers. This issue is tackled by introducing a chemically aware strategy for the Unitary Coupled Cluster ansatz. The objective is to use the chemical description of a system to aid in the synthesis of a quantum circuit. We combine this approach with two flavours of Symmetry Verification for the reduction of experimental noise. These methods enable the use of System Model H1 for a 6-qubit Quantum Subspace Expansion calculation. We present (i) calculations to obtain methane's optical spectra; (ii) an atmospheric gas reaction simulation involving $[\text{CH}_3 - \text{H} - \text{OH}]^\ddagger$. Using our chemically aware unitary coupled cluster state-preparation strategy in tandem with state of the art symmetry verification methods, we improve device yield for CH_4 at 6-qubits. This is demonstrated by a 90% improvement in two-qubit gate count and reduction in relative error to 0.2% for electronic energy calculated on System Model H1.

Keywords: Quantum Computation · Unitary Coupled Cluster · UV/ VIS Spectra · Quantum Subspace Expansion

The simulation of molecules and materials using quantum chemistry methods is a well established field, with applications in many scientific and industrial areas of interest [1]. However, there is awareness about the shortcomings of performing these simulations on classical machines [2]. The main workhorse of classical simulations, Density Functional Theory, fails to capture the qualitative behaviour of chemicals with strong correlation [3]. One naturally turns to wave function methods, such as Hartree-Fock (HF), Coupled Cluster (CC) theory and Configuration Interaction (CI) methods. However, the steep memory requirements of these techniques have limited their practicality in the study of complex chemicals. This issue also plagues classical excited state heuristics that provide CI- or CCSD-like accuracy. For instance, Equation of Motion Coupled Cluster (EOM-CCSD) scales as $O(N^6)$, where N is the number of spin orbitals [4].

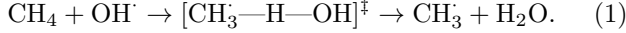
Quantum computers provide an alternative path to enable the use of wave function methods on problems of practical interest. In particular, two state of the art algorithms have been proposed, the Variational Quantum Eigensolver (VQE) and Quantum Subspace Expansion (QSE) algorithms, as the earliest candidates for scalable alternatives to classical wave function methods [5, 6, 7]. VQE approximates the ground-state of a Hamiltonian variationally, and QSE estimates excited states non-variationally. Despite the rapid development and deployment of quantum resources, progress has been limited due to quantum hardware being unable to meet performance requirements of these algorithms. Neverthe-

less, the exploration of quantum computing applications for chemistry is necessary for the progression of computational chemistry, and also serve as important benchmarks for today's hardware and its relevance to the chemicals industry.

Quantum algorithms for chemistry require a large amount of quantum resources for the state-preparation component of these simulations. Broadly, two families of state-preparation methods have been introduced in literature: Unitary Coupled Cluster (UCC), and hardware-efficient ansätze. With UCC, the number of variational circuit parameters and the 2-qubit gate depth scale as $O(N^4)$, leading to circuits beyond the capability of today's machines [8]. Hardware-efficient methods require less coherent resources, but suffer from the "barren plateau" problem [9]. Initial effort has been focused on improving the 2-qubit depth scaling for the UCC ansatz. Notably, adaptive methods [10], circuit recompilation [11], and unique UCC circuit synthesis approaches [12]. Adaptive methods are unattractive. For example, ADAPT-VQE requires additional measurements on top of regular VQE [13]. This encourages us to explore a unique UCC circuit synthesis approach that improved the 2-qubit gate count by describing Fermionic UCC spatial orbital to spatial orbital excitations as hard-core Bosonic operators [14, 15, 16]. In tandem, there has been additional work on discarding UCC excitations by using symmetry filtering a priori [17, 18], also resulting in lower two-qubit gate count.

One particular example where quantum computing can help is the simulation of refrigerants. The design of novel re-

frigerants has proven challenging due to trade-offs in key molecular properties such as global warming potential and ozone depletion potential, whilst also considering other properties such as toxicity, flammability, and stability. As such, molecular simulations have become increasingly used for investigating the structure-activity relationship of candidate refrigerants [19]. As a test case, we consider methane (CH_4) and its reaction with the hydroxyl radical (OH^\cdot),



CH_4 's atmospheric properties have been thoroughly studied [20] and can provide guidelines in the application of quantum computers for search of new environment-friendly refrigerants. In order to characterise this process, one also needs to calculate a series of energies corresponding to the products, methyl radical (CH_3^\cdot) and water (H_2O). To estimate the reaction barrier that governs the kinetics of the reaction, we also simulate the transition state, $[\text{CH}_3\text{—H—OH}]^\ddagger$.

In Section II, we give a detailed overview combining excitation filtering based on Z_2 symmetries, hard-core Boson representation, and favourable two-qubit gate cancellation (via Pauli-gadget synthesis scheme of Ref. [21]). Section III is devoted to the results obtained with our state-preparation strategy on System Model H1, powered by Honeywell. We focus on the resource reduction, and consider noisy calculations for CH_4 's optical spectra. Finally, we complete our investigation with a simulation of $[\text{CH}_3\text{—H—OH}]^\ddagger$ and other reaction participants. We also apply symmetry verification to our calculations [22]. The two symmetry verification techniques we use are Partition Measurement Symmetry Verification (PMSV) and Mid-circuit Measurement Symmetry Verification (MMSV) [23].

1 Methods

1.1 Chemically Aware Unitary Coupled Cluster

For our state-preparation strategy, we use Jordan-Wigner Encoding (JWE) to map Trotterised Fermionic exponents to Pauli operators acting on qubits [24, 25]. We refer to the by-product sequence of Pauli-Z operations as JWE-strings, which consequently increase the effective k -locality of UCC exponents. Our spin orbitals and therefore the qubit register have alpha-beta ordering (each even-odd indexed spin orbital corresponds to a spatial orbital). Appendix A has more information on the UCC state-preparation method and conventional circuit decompositions (Individual and Commuting Sets synthesis). The steps of the chemically aware strategy are as follows:

I. Symmetry Filtering: Filter the set of excitations composing the ansatz via use of molecular symmetry to identify forbidden terms. We used two techniques:

- (a) Defining Z_2 symmetries to check commutation against the UCC excitation operators [26, 27, 17];
- (b) A point group symmetry filtering method for CCSD adapted to be used for UCCSD [28].

II. Spatial Orbital to Spatial Orbital: There are three steps to compactly describe a pair of electrons excited between spatial orbitals. For this method, we necessarily change the ordering of the excitations to benefit from the two-qubit gate savings associated with spatial to spatial UCC excitation.

- (a) **Specify Double Occupied Spatial Orbitals:** Only doubly occupied ($|1\rangle$) and virtual spatial orbitals ($|0\rangle$) are considered. For example, the Hartree-Fock state $|111000\rangle$ defining molecular spin orbital occupation, would be processed to return $|100\rangle$ in the molecular spatial orbital occupation. These occupations are mapped to the even-indexed qubits on the circuit, $|100000\rangle$. Single occupied spatial orbitals are ignored.
- (b) **Hard-core Boson Representation:** Operations that excite a pair electrons from and to the same spatial orbital can be synthesised more efficiently. These excitations are of the type:

$$\hat{a}_{2p}^\dagger \hat{a}_{2q} \hat{a}_{2p+1}^\dagger \hat{a}_{2q+1} - h.c., \quad (2)$$

where $q < p$, and both variables track the spatial orbital index. Applying JWE results in 8 unique Pauli exponents over 4-qubits.

These excitations lack JWE-strings, signifying zero parity exchange as these adjacent electrons hop between different spatial orbitals. It can be seen that these excitations act on spin-orbitals, but excite and de-excite electrons between spatial orbitals. These adjacent electrons travel together, yet cannot occupy the same spatial orbital with another pair of electrons. Equation 2 can also be expressed as,

$$\hat{b}_p^\dagger \hat{b}_q - h.c., \quad (3)$$

where \hat{b} denotes a Hard-core Bosonic operation. Eq. 3 can be re-expressed by using the equivalence between Hard-core Bosons and Pauli operations [29, 30],

$$\frac{1}{2} \left\{ \hat{Y}_q \hat{X}_p - \hat{X}_q \hat{Y}_p \right\}. \quad (4)$$

We relabel the indices of equation 4 from $p \rightarrow 2p$ and $q \rightarrow 2q$. Each of these spatial orbital to spatial orbital excitations act on 2 qubits and require 2 two-qubit gates.

- (c) **Introduce Spin Orbitals:** We apply two-qubit gates on relevant even-odd qubits. Each even-indexed qubit corresponds to the alpha spin-orbital of a spatial orbital, and similarly each beta spin-orbital is represented by an odd-indexed qubit. Single occupation of a spatial orbital is included by initializing the relevant alpha-index qubit to the $|1\rangle$ state.

III. Commuting sets of Pauli strings: The remaining double and single excitations are synthesised. Each double excitation contains 8 Pauli-sub terms and these terms naturally form a commuting set. We synthesise these excitations in commuting sets with tket, resulting in 14 two-qubit gates

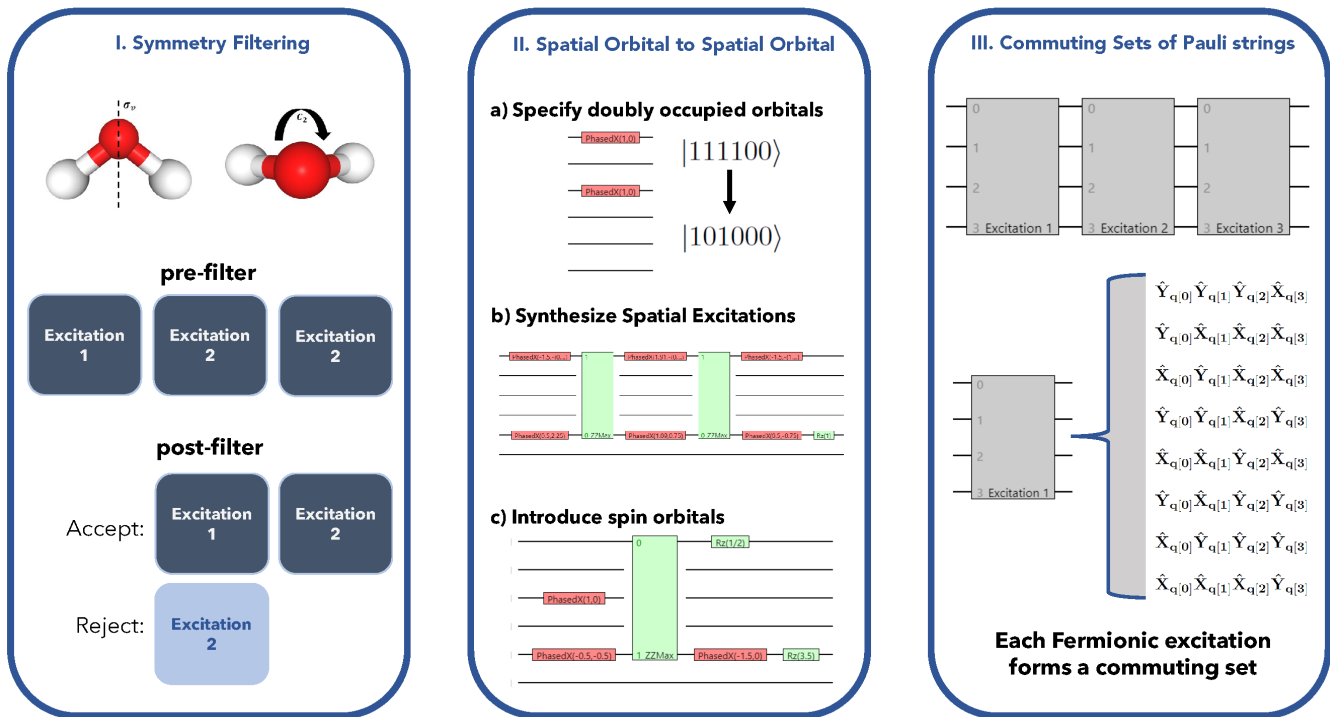


Fig. 1. Schematic showing three major steps of the chemically aware ucc state-preparation strategy. Step (i) uses symmetry as a priori to discard excitations. Step (ii) is a compact synthesis scheme for spatial to spatial excitations. Step (iii) uses tket to synthesise generic double and single excitations by commuting sets to maximize pauli-string cancellation. Each single or double UCC excitation is naturally a commuting set of Pauli-strings.

at best. Increasing the length of JWE-strings increases the number of two-qubit gates for the corresponding decomposition. Circuits for single fermionic excitations contain at minimum four two-qubit gates and act over 3 qubits. Both two-qubit gate count and number of qubits grow as the number of Pauli-Z strings increase.

2 Results

All the circuits in this paper are prepared using Quantinuum’s quantum chemistry package InQuanto [31, 32]. The integrals to obtain the relevant chemistry Hamiltonians were obtained using an InQuanto extension to the open-source chemistry software package, PySCF, known as InQuanto-PySCF [33]. InQuanto provides the tools provide the pre- & post-processing logic to perform quantum computation, and more importantly to map the results from quantum computation back to the Chemistry problem. The UCC state-preparation techniques used in this paper are available in InQuanto. NGLView is used to visualize chemical structures and molecular orbitals via an InQuanto interface. We use the open-source ADCC library to compute benchmark optical spectra data at ADC-2 level of theory, [34].

For this investigation, we used system model H1 devices and emulators [35, 36]. The IBMQ *qasm* simulator was used to perform noiseless state-vector calculations, simulations with finite sampling noise and zero quantum noise. We use tket to synthesise, optimize and retarget quantum circuits to enable execution on a H1 hardware [37, 38].

All our benchmark calculation are non-variational operator averaging calculations (Hamiltonian Averaging or QSE). The ground-state parameters for our state-preparation circuits are obtained via a noiseless VQE qasm simulation.

2.1 Improvements due to the Chemically Aware Strategy

We investigate the two-qubit gate count across three different methods, chemically aware, commuting sets, and individual UCCSD synthesis. We use CH_4 at equilibrium geometry as a benchmark system, alongside the D_2 point group to describe the molecular orbital symmetry [39]. Fig. 2a reports an improvement by approximately 81% (commuting sets) and 95% (individual) in two-qubit gate count for various active-spaces ranging from 4 qubits to 18 qubits. By neglecting symmetry (C_1 point group), we reduce the efficacy of chemically aware to reduce two-qubit gate count, rendering only a small improvement due to the compact spatial-orbital-only excitation synthesis. Fig. 2b does not report any improvement in overall scaling with chemically aware compared to commuting sets synthesis for CH_4 with C_1 symmetry.

ADAPT-VQE improves upon individual synthesis by iteratively constructing a compact ansatz. At the cost of increasing the total number of measurements, ADAPT discards both symmetry-forbidden and minimally contributing symmetry-allowed excitations. As a consequence, ADAPT circuits have a lower two-qubit gate count. With the chem-

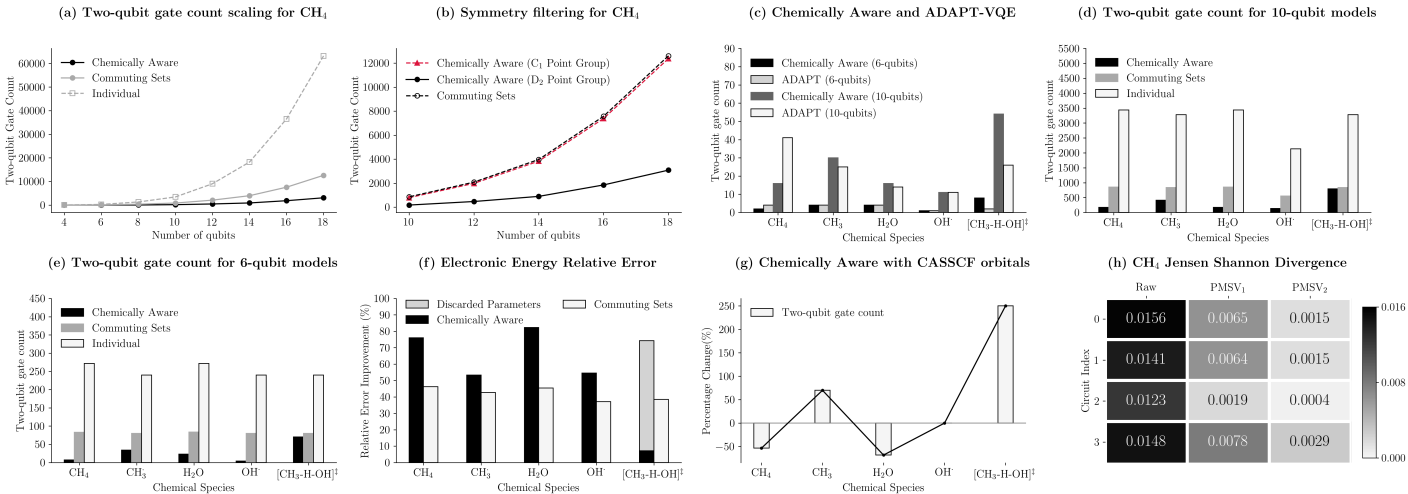


Fig. 2. (a): Two-qubit gate count scaling for various CH₄ active spaces. (b) Role of symmetry in two-qubit gate count improvement coming from chemically aware. Test case CH₄ with D₂ point group. (c) Comparison of excitation filtering in ADAPT compared to chemically aware for 10-qubit and 6-qubit models. (d) Two-qubit gate count comparison between chemically aware strategy, commuting sets and individual synthesis circuits with symbolic gates for 10-qubits and (e) 6-qubits. (f) Improvement in relative error on ground-state energy on H1-1E for chemically aware (commuting sets) compared to individual synthesis. (g) Two-qubit gate count improvement using chemically aware over commuting sets for CASSCF optimised 6-qubit models. (h) Jensen-Shannon Divergence for measurement statistics per simulated chemically aware CH₄ circuit (indexed between 0 and 3) on H1-2 for three experiments. Raw is a sampling experiment with no error mitigation, PMSV₁ is use of total electron conservation to post-select measurement results, and PMSV₂ is use of all U₁ (alpha- and beta-electron number conservation) and Z₂ operators (two symmetric transformations coming from point group of MOs).

ically aware strategy, we bypass ADAPT’s extra measurement cost to improve two-qubit gate count. Fig. 2c shows the number of Fermionic excitations with chemically aware compared to ADAPT. For symmetric molecules, ADAPT approximately returns a similar number of Fermionic excitations as chemically aware for both 6-qubit and 10-qubit active spaces. For [CH₃-H-OH][‡], a 75% (6-qubits) and 50% (10-qubits) improvement in the number of excitations is observed. We attribute it to: (i) Additional symmetry in [CH₃-H-OH][‡] not exploited by chemically aware; (ii) ADAPT discards symmetry-allowed excitations of minimal contribution to the “true” ground state.

For 10-qubit and 6-qubit models from Eq. 1, we show empirical improvement in chemically aware two-qubit count compared to statistics from benchmark methods (commuting sets and individual). The two-qubit gate counts provided are for circuits with arbitrary phase gates with symbolic rotation parameters, hence independent from parameter sets characterizing specific physical states. Excluding the transition state and CH₃, chemically aware improves upon commuting sets by 75%-80% (10-qubits) and 70%-95% (6-qubits). For less symmetric species, CH₃ and [CH₃-H-OH][‡], we observe a less drastic two-qubit gate improvement with chemically aware.

With chemically aware state-preparation, we expect to see lower error in electronic energy compared to calculations using commuting sets synthesis. We compare improvement in relative error using the chemically aware strategy (commuting sets synthesis) compared to individual synthesis at ground-state parameters on the H1 emulator (H1-1E). Excluding the transition state, Fig. 2f reports substantial improvement. For [CH₃-H-OH][‡], chemically aware offers

less improvement (7%) compared to commuting sets (38%). We note that tket defines arbitrary-phase gates as redundant for rotations below the 1×10^{-12} threshold. The parameter set for commuting sets synthesised circuits (27 two-qubit gates) contains angles of size 10^{-30} . For the chemically aware circuit (60 two-qubit gates), the smallest parameters are of magnitude 10^{-7} . Discarding parameters smaller than 1×10^{-3} has a negligible impact on the electronic ground state energy, and we observe an improvement (74%) in the chemically aware calculation (16 two-qubit gate count).

Since we are using active space models, we also need to relax the molecular orbital coefficients within the defined active space via a Complete Active Space SCF (CASSCF) routine. This aids in better recovery of electronic correlation with VQE methods. Fig. 2g reports the two-qubit gate count increase for chemically aware when using CASSCF orbitals over SCF orbitals at ground-state parameters. We only see an increase in two-qubit gate depth for CH₃ and the transition state, mainly due to increase in the number of non-negligible UCC parameters (greater than 10^{-3}). This leads to less excitations being redundant and therefore more two-qubit gates. All species (excluding OH) report varying degrees of improvement in electronic correlation recovery.

We perform Hamiltonian averaging experiments for 6-qubit CH₄ with D₂ symmetry using (i) no error mitigation, (ii) PMSV with a U₁ symmetry constraint (total electron conservation) and (iii) with alpha- and beta-number conservation and Point group operations defined as Z₂ symmetries. We require 4 circuits to measure the electronic energy. Tab. 5 in Appendix E reports improvement in relative error as we add more constraints to PMSV. Fig. 2h shows improvement in Jensen-Shannon Divergence (JSD) by one order of mag-

nitude after PMSV application. We simulate a CH_4 circuit with 500 shots to generate measurement statistics on H1-2. The distribution of outcomes is compared with output from a noiseless qasm simulator. A JSD with value zero means experimental measurement distribution exactly agrees with theory data. After PMSV₂ application (see Fig. 2g for definition), we observe a JSD value of magnitude 10^{-3} .

2.2 Excited States & Optical Spectra

In order to improve feasibility for hardware, we employed a set of nearly orthonormal custom expansion operators. We observe a drastic reduction of resources at the cost of finding only a subset of singlet states and zero triplet states. Using a near orthonormal set of expansion operators causes less error to accumulate in the overlap quantity, S , of the QSE equation, $Hc = eSc$. We use a circuit with 7 two-qubit gates and sample 31 measurement circuits 500 times each. Tab. 1 successfully reports 4 out of 5 excitation energies. Each excitation is defined from the singlet ground-state, S_0 , to a singlet excited state, S_n . We use total-electron number conservation as a constraint to post-select on the measurement results. We find the penalty of adding extra two-qubit gates renders MMSV ineffective, giving a similar level of accuracy as the experiment with no error mitigation (Raw). PMSV is effective at reducing ground state deviation. Similar to the Hamiltonian averaging procedure, using more symmetry constraints (PMSV₂) improves accuracy of the computed quantity. With PMSV₂, we are able to replicate degeneracy between S_2 and S_3 (to three decimal places). We note with PMSV application, the excitation energies are increasing overestimated from S_1 to S_4 .

Table 1. Excitation energies from ground state singlet, S_0 , to the first four excited states, S_n , where $n = \{0, 1, 2, 3, 4, 5\}$ QSE calculation on CH_4 at equilibrium geometry on H1-2 hardware. MMSV, PMSV₁ and PMSV₂ used to mitigate errors. EOM is EOM-CCSD with intel x86_64 processor.

	MMSV (Ha)	PMSV ₁ (Ha)	PMSV ₂ (Ha)	Raw (Ha)	EOM (Ha)
$S_0 \rightarrow S_1$	0.837	0.843	0.868	0.836	0.862
$S_0 \rightarrow S_2$	0.854	0.852	0.868	0.848	0.862
$S_0 \rightarrow S_3$	1.616	1.617	1.639	1.608	1.634
$S_0 \rightarrow S_4$	1.718	1.735	1.749	1.724	1.715
$S_0 \rightarrow S_5$	-	-	-	-	1.740

After performing the QSE computation, we obtain a description of a set of excited states,

$$|\psi_v\rangle = \sum_k w_k^v \hat{F}_k |\psi_0\rangle, \quad (5)$$

where $|\psi_0\rangle$ is the ground-state, w_k^v is a coefficient vector for the v^{th} excited state found with QSE and \hat{F}_k are the corresponding QSE expansion operators (i.e. $\hat{a}_2^\dagger \hat{a}_0$). With this information post-QSE procedure, one can cast an overlap, $\langle \psi_0 | \psi_v \rangle$, into a sequence of operator averaging procedures, $\sum_k \langle \psi_0 | w_k^v \hat{F}_k |\psi_0\rangle$. This is extremely useful for evaluating quantities needed to obtain optical spectra, i.e. transition density matrices and transition dipole moments.

Our intention is to obtain optical spectra with the QSE result. We use dipole operators, $\hat{\mu}_\alpha$, with $\alpha = (x, y, z)$ and the

origin as the charge centre. A post-QSE operator averaging procedure is performed to obtain transition dipole moments for each of the singlet states, $\langle \psi_0 | \hat{\mu}_\alpha | \psi_v \rangle$, using Eq. 5 to absorb the QSE expansion operators into $\hat{\mu}_\alpha$. The oscillator strength, f , can be obtained as a post-processing procedure,

$$f = \frac{2\epsilon_v}{3} \sum_{\alpha=\{x,y,z\}} |\langle \psi_0 | \hat{\mu}_\alpha | \psi_v \rangle|^2, \quad (6)$$

where ϵ_v is the transition energy from state $|\psi_0\rangle$ to $|\psi_v\rangle$.

Fig. 3 reports optical spectra data computed with H1-2 hardware. A subsequent transition dipole moment calculation was performed on H1-2 with 500 shots per circuit. Comparing with noiseless qasm simulations as a benchmark, there is one peak at 0.86 Ha (oscillator strength 0.59). This peak corresponds to two degenerate states. The H1-2 quantum computer produces two peaks very close at 0.8676 Ha (oscillator strength 0.601) and 0.8684 Ha (oscillator strength 0.565). This small discrepancy between two degenerate states is added primarily by sampling noise.

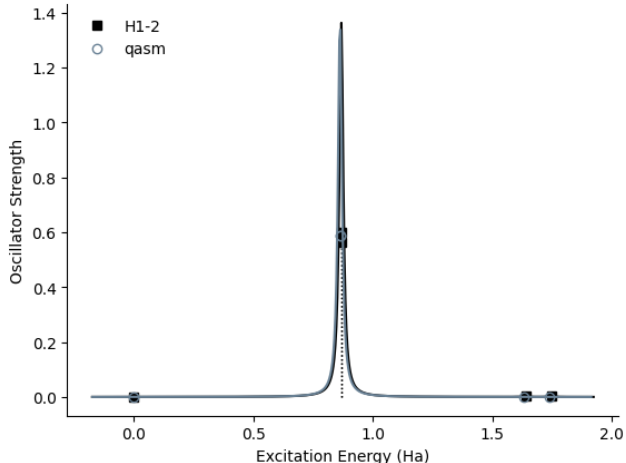


Fig. 3. Optical spectra calculated with H1-2 hardware (black squares) and noiseless qasm simulator (blue circles). Black line is Lorentzian line broadening.

2.3 Atmospheric Reaction Simulation

After presenting our results for the characterization of the methane molecule, we proceed now to show our results for the simulation of the $\text{CH}_4 + \text{OH} \rightarrow \text{CH}_3 + \text{H}_2\text{O}$ reaction. We focus first on the thermodynamics of reactants and products, and then proceed to analyse our results for the transition state and the activation energy for the reaction. Here, we present our results for 6-qubit active space models, which are suitable for experiments on hardware.

The results for the activation energy of the reaction are shown in Table 2. The absolute value of the energy differences is too small to be reproduced, which can be seen from the results of the noiseless simulation. The main reason for this is the small number of qubits considered and, as a consequence, insufficient accuracy for each of the species participating in the reaction. As a result, in a hardware experiment the activation energy is found to be negative,

although the order of magnitude of its absolute value is correct for the latter. This result is an indicator of the general difficulty of accurately calculating reaction barriers, due to the small energy differences involved and large accuracy required. To our knowledge, this is the first time an activation energy has been calculated on an actual ion trap hardware although theoretical work estimating reaction energy profiles using much larger numbers of qubits exist [41].

Table 2. Activation energy for the reaction between methane and the hydroxyl radical (AE), and for the reverse process (R-AE).

	Ref. [40] (Ha)	qasm (Ha)	H1-1 (Ha)
AE	+0.01	+0.12	-0.05
R-AE	+0.02	+0.12	+0.01

3 Discussion

In this work, we have: (a) improved UCC circuit synthesis to reduce two-qubit gate count, (b) performed a 6-qubit QSE calculation on System Model H1 to output optical spectra (c) estimated the reaction barrier from Eq. 1.

Alongside the two-qubit gate savings from state-preparation, the PMSV error mitigation technique has allowed us to significantly improve the quality of the energy calculations by reducing absolute error on the ground-state energy. For CH_4 and OH^\cdot , the results are in strong agreement with state-vector simulations. Alongside the 6-qubit QSE calculation showcased by Ref. [42] on a superconducting IBMQ quantum computer, we have performed a 6-qubit excited states calculation for methane on ion-trap hardware (System Model H1), advancing the industry-standard of using “4 qubits or less” [43]. We note that symmetry-verification is applicable to small molecules with number conservation properties and mirror-planes, and should be useful for relevant future experiments. However, we note the efficacy of PMSV may deteriorate as we scale to larger, more non-symmetric molecules that require a greater number of qubits. The long term need for error correction still exists.

We also employed H1’s mid-circuit measurement facility to symmetry verify our calculation results. Whilst outperformed by PMSV, it is still inconclusive to exclude the use of mid-circuit measurements. We believe this functionality still has more applications for hardware chemistry experiments, i.e. approximating required quantities in variational real time evolution.

Computation of chemical quantities, such as UV/VS spectra is essential for comparison with experimental data. We use the QSE description of the excited states to evaluate transition dipole moments and ultimately optical spectra. We learn optical spectra quality depends on excitation energy accuracy of the prior QSE procedure. Most importantly, we control sampling error from the prior QSE procedure, by choosing select single and double UCC excitations, albeit at the cost of restricting to a subset of singlet excited states.

From our investigation to compute the reaction barrier, we learn that dynamical correlation is difficult to recover on

today’s quantum computers. This is especially important when the energy difference between the reactants, products, and transition states are expected to be small. Specifically, to recover correlation for $[\text{CH}_3\text{—H—OH}]^\ddagger$, many orbitals are needed. With chemically aware UCC Synthesis, the decrease in two-qubit gate count was not as dramatic as the other species, due to molecular asymmetry. A slight improvement in two-qubit gate count is observed and is outperformed by Fermionic ADAPT VQE. We believe that there maybe additional unexploited redundancy in our model of $[\text{CH}_3\text{—H—OH}]^\ddagger$. However, the possibility remains that ADAPT discards symmetry-allowed unimportant excitations. Further analysis is needed to investigate this and to determine if the filtering by ADAPT can be performed a priori on a classical computer. We also did not investigate the use of ADAPT-VQE as a second UCC excitation filter in the chemically aware strategy. We dedicate future work towards this effort.

4 Conclusion

We incrementally extend the reach of quantum computation by performing the QSE algorithm to obtain chemically relevant quantities such as optical spectra. Open questions remain in the use of QSE to obtain vibrational or infrared spectra.

Alongside two-qubit gate count, the number of measurements is a major bottleneck preventing scaling beyond 10-qubits. We have identified the need to drastically reduce the cost of the operator averaging procedure, which is used in VQE and QSE. Follow-up analysis of newer measurement methods is necessary [44, 45]. We additionally believe that run-time requirements and accuracy for QSE can be reduced by application of point-group symmetry. This is done similarly for EOM-CCSD, and the application to QSE needs to be investigated in detail.

To summarize, we have showed in this paper a series of techniques to help extract the maximum yield from current and near-term hardware. We anticipate that these techniques will help enable future small chemistry experiments on quantum devices on near-term hardware.

Acknowledgements

We would like to thank Quantinuum’s hardware & software units for discussions surrounding excited state chemistry, experiment design, results analysis and device access. Specifically, we thank Michal Krompiec, David Zsolt Manrique, Kentaro Yamamoto, Jenni Strabley, Brian Neyenhuis, Simon McAdams, Ross Duncan, Seyon Sivarajah, John Children, Silas Dilkes, Alec Edgington, Sam White, Isobel Hooper, Andrew Tranter, Moshin Iqbal, Henrik Dreyer & Gavin Towler. We are also grateful to Joaquin Espinosa-Garcia and Jose C. Corchado for providing the geometrical configuration for $[\text{CH}_3\text{—H—OH}]^\ddagger$. We appreciate positively the support provided by Honeywell Performance Materials & Technology (PMT).

Author Contributions

I. T. Khan developed and investigated the chemically aware circuit state-preparation, and its application to refrigerant molecules. I. T. K also evaluated optical spectra via Quantum

Subspace Expansion on System Model H1. **M. Tudorovskaya** performed the reaction barrier study with calculations on System Model H1. **J. J. M. Kirsopp** implemented point group filtering from Ref. [28]. **D. Muñoz Ramo** provided technical oversight on the relevance and application of the methods outlined in this paper to the problem of atmospheric refrigerants. **P. Warrior, D. K. Papanastasiou & R. Singh** defined the atmospheric refrigerants use-case, and provided oversight on application and relevance to quantum computing.

Availability of Data and Materials

Data is available upon request from authors. All inquiries regarding the InQuanto Platform should be made to inquanto-support@quantinuum.com.

Correspondence

Queries and requests should be addressed to Irfan T. Khan (irfan.khan@quantinuum.com), or David Muñoz Ramo (david.munozramo@quantinuum.com).

Competing Interests

We declare the use of Quantinuum H-Series devices & the IBMQ *qasm* simulator. The views expressed in this paper do not reflect the official policy or position of IBM, Honeywell International and any related subsidiaries. IBM and Honeywell International are also Quantinuum shareholders.

References

- [1] W. Kohn. Nobel lecture: Electronic structure of matter—wave functions and density functionals. *Rev. Mod. Phys.*, 71:1253–1266, Oct 1999. doi: 10.1103/RevModPhys.71.1253. URL <https://link.aps.org/doi/10.1103/RevModPhys.71.1253>.
- [2] Yudong Cao, Jonathan Romero, Jonathan P. Olson, Matthias Degroote, Peter D. Johnson, Mária Kieferová, Ian D. Kivlichan, Tim Menke, Borja Peropadre, Nicolas P. D. Sawaya, Sukin Sim, Libor Veis, and Alán Aspuru-Guzik. Quantum chemistry in the age of quantum computing. *Chemical Reviews*, 119(19):10856–10915, aug 2019. doi: 10.1021/acs.chemrev.8b00803. URL <https://doi.org/10.1021%2Facs.chemrev.8b00803>.
- [3] Axel D. Becke. Perspective: Fifty years of density-functional theory in chemical physics. *The Journal of Chemical Physics*, 140(18):18A301, 2014. doi: 10.1063/1.4869598. URL <https://doi.org/10.1063/1.4869598>.
- [4] Hideo Sekino and Rodney J. Bartlett. A linear response, coupled-cluster theory for excitation energy. *International Journal of Quantum Chemistry*, 26(S18):255–265, 1984. doi: <https://doi.org/10.1002/qua.560260826>. URL <https://onlinelibrary.wiley.com/doi/abs/10.1002/qua.560260826>.
- [5] Alberto Peruzzo, Jarrod McClean, Peter Shadbolt, Man-Hong Yung, Xiao-Qi Zhou, Peter J. Love, Alán Aspuru-Guzik, and Jeremy L. O’Brien. A variational eigenvalue solver on a photonic quantum processor. *Nature Communications*, 5(1), Jul 2014. ISSN 2041-1723. doi: 10.1038/ncomms5213. URL <http://dx.doi.org/10.1038/ncomms5213>.
- [6] Abhinav Kandala, Antonio Mezzacapo, Kristan Temme, Maika Takita, Markus Brink, Jerry M. Chow, and Jay M. Gambetta. Hardware-efficient variational quantum eigensolver for small molecules and quantum magnets. *Nature*, 549(7671):242–246, Sep 2017. ISSN 1476-4687. doi: 10.1038/nature23879. URL <http://dx.doi.org/10.1038/nature23879>.
- [7] Jarrod R. McClean, Mollie E. Kimchi-Schwartz, Jonathan Carter, and Wibe A. de Jong. Hybrid quantum-classical hierarchy for mitigation of decoherence and determination of excited states. *Physical Review A*, 95(4), Apr 2017. ISSN 2469-9934. doi: 10.1103/physreva.95.042308. URL <http://dx.doi.org/10.1103/PhysRevA.95.042308>.
- [8] Jarrod R McClean, Jonathan Romero, Ryan Babbush, and Alán Aspuru-Guzik. The theory of variational hybrid quantum-classical algorithms. *New Journal of Physics*, 18(2):023023, Feb 2016. ISSN 1367-2630. doi: 10.1088/1367-2630/18/2/023023. URL <http://dx.doi.org/10.1088/1367-2630/18/2/023023>.
- [9] Jarrod R. McClean, Sergio Boixo, Vadim N. Smelyanskiy, Ryan Babbush, and Hartmut Neven. Barren plateaus in quantum neural network training landscapes. *Nature Communications*, 9(1):4812, Nov 2018. ISSN 2041-1723. doi: 10.1038/s41467-018-07090-4. URL <https://doi.org/10.1038/s41467-018-07090-4>.
- [10] Ilya G. Ryabinkin, Tzu-Ching Yen, Scott N. Genin, and Artur F. Izmaylov. Qubit coupled-cluster method: A systematic approach to quantum chemistry on a quantum computer, 2018. URL <https://arxiv.org/abs/1809.03827>.
- [11] Tyson Jones and Simon C. Benjamin. Robust quantum compilation and circuit optimisation via energy minimisation. *Quantum*, 6:628, January 2022. ISSN 2521-327X. doi: 10.22331/q-2022-01-24-628. URL <https://doi.org/10.22331/q-2022-01-24-628>.
- [12] Alexander Cowtan, Silas Dilkes, Ross Duncan, Will Simmons, and Seyon Sivarajah. Phase gadget synthesis for shallow circuits. *Electronic Proceedings in Theoretical Computer Science*, 318:213–228, May 2020. ISSN 2075-2180. doi: 10.4204/eptcs.318.13. URL <http://dx.doi.org/10.4204/EPTCS.318.13>.
- [13] Harper R. Grimsley, Sophia E. Economou, Edwin Barnes, and Nicholas J. Mayhall. An adaptive variational algorithm for exact molecular simulations on a quantum computer. *Nature Communications*, 10(1), jul 2019. doi: 10.1038/s41467-019-10988-2. URL <https://doi.org/10.1038%2Fs41467-019-10988-2>.
- [14] Yunseong Nam, Jwo-Sy Chen, Neal C. Pienti, Kenneth Wright, Conor Delaney, Dmitri Maslov, Kenneth R. Brown, Stewart Allen, Jason M. Amini, Joel Apisdorf, Kristin M. Beck, Aleksey Blinov, Vandiver Chaplin, Mika Chmielewski, Coleman Collins, Shantanu Debnath, Andrew M. Ducre, Kai M. Hudek, Matthew Keesan, Sarah M. Kreike-meier, Jonathan Mizrahi, Phil Solomon, Mike Williams, Jaime David Wong-Campos, Christopher Monroe, and Jungsang Kim. Ground-state energy estimation of the water molecule on a trapped ion quantum computer, 2019.
- [15] Jakob S. Kottmann and Alán Aspuru-Guzik. Optimized low-depth quantum circuits for molecular electronic structure using a separable-pair approximation. *Physical Review A*, 105(3), mar 2022. doi: 10.1103/physreva.105.032449. URL <https://doi.org/10.1103%2Fphysreva.105.032449>.
- [16] Vincent E. Elfving, Marta Millaruelo, José A. Gámez, and Christian Gogolin. Simulating quantum chemistry in the seniority-zero space on qubit-based quantum computers. *Physical Review A*, 103(3), mar 2021. doi: 10.1103/physreva.103.032605. URL <https://doi.org/10.1103%2Fphysreva.103.032605>.
- [17] David Zsolt Manrique, Irfan T. Khan, Kentaro Yamamoto, Vijja Wichitwechkarn, and David Muñoz Ramo. Momentum-space unitary coupled cluster and translational

- quantum subspace expansion for periodic systems on quantum computers, 2020. URL <https://arxiv.org/abs/2008.08694>.
- [18] Changsu Cao, Jiaqi Hu, Wengang Zhang, Xusheng Xu, Dechin Chen, Fan Yu, Jun Li, Hanshi Hu, Dingshun Lv, and Man-Hong Yung. Towards a larger molecular simulation on the quantum computer: Up to 28 qubits systems accelerated by point group symmetry, 2021. URL <https://arxiv.org/abs/2109.02110>.
- [19] Partha P. Bera, Joseph S. Francisco, and Timothy J. Lee. Design strategies to minimize the radiative efficiency of global warming molecules. *Proceedings of the National Academy of Sciences*, 107(20):9049–9054, 2010. doi: 10.1073/pnas.0913590107. URL <https://www.pnas.org/doi/abs/10.1073/pnas.0913590107>.
- [20] Donald J Wuebbles and Katharine Hayhoe. Atmospheric methane and global change. *Earth-Science Reviews*, 57(3):177–210, 2002. ISSN 0012-8252. doi: [https://doi.org/10.1016/S0012-8252\(01\)00062-9](https://doi.org/10.1016/S0012-8252(01)00062-9). URL <https://www.sciencedirect.com/science/article/pii/S0012825201000629>.
- [21] Alexander Cowtan, Will Simmons, and Ross Duncan. A generic compilation strategy for the unitary coupled cluster ansatz, 2020.
- [22] Kentaro Yamamoto, David Zsolt Manrique, Irfan Khan, Hideaki Sawada, and David Muñoz Ramo. Quantum hardware calculations of periodic systems with partition-measurement symmetry verification: simplified models of hydrogen chain and iron crystals, 2021. URL <https://arxiv.org/abs/2109.08401>.
- [23] X. Bonet-Monroig, R. Sagastizabal, M. Singh, and T. E. O’Brien. Low-cost error mitigation by symmetry verification. *Physical Review A*, 98(6), Dec 2018. ISSN 2469-9934. doi: 10.1103/physreva.98.062339. URL <http://dx.doi.org/10.1103/PhysRevA.98.062339>.
- [24] E Wigner and Pascual Jordan. Über das paulische äquivalenzverbot. *Z. Phys*, 47:631, 1928.
- [25] L.-A. Wu, M. S. Byrd, and D. A. Lidar. Polynomial-time simulation of pairing models on a quantum computer. *Phys. Rev. Lett.*, 89:057904, Jul 2002. doi: 10.1103/PhysRevLett.89.057904. URL <https://link.aps.org/doi/10.1103/PhysRevLett.89.057904>.
- [26] Tzu-Ching Yen, Robert A. Lang, and Artur F. Izmaylov. Exact and approximate symmetry projectors for the electronic structure problem on a quantum computer. *The Journal of Chemical Physics*, 151(16):164111, Oct 2019. ISSN 1089-7690. doi: 10.1063/1.5110682. URL <http://dx.doi.org/10.1063/1.5110682>.
- [27] Kanav Setia, Richard Chen, Julia E. Rice, Antonio Mezzacapo, Marco Pistoia, and James Whitfield. Reducing qubit requirements for quantum simulation using molecular point group symmetries, 2020.
- [28] Petr Čárský, Lawrence J. Schaad, B. Andes Hess, Miroslav Urban, and Jozef Noga. Use of molecular symmetry in coupled-cluster theory. *The Journal of Chemical Physics*, 87(1):411–415, 1987. doi: 10.1063/1.453585. URL <https://doi.org/10.1063/1.453585>.
- [29] Takeo Matsubara and Hirotsugu Matsuda. A Lattice Model of Liquid Helium, I. *Progress of Theoretical Physics*, 16(6): 569–582, 12 1956. ISSN 0033-068X. doi: 10.1143/PTP.16.569. URL <https://doi.org/10.1143/PTP.16.569>.
- [30] E. G. Batyev and L. S. Braginskii. Antiferromagnet in a strong magnetic field: analogy with Bose gas. *Soviet Journal of Experimental and Theoretical Physics*, 60(4):781, October 1984.
- [31] Andrew Tranter, Cono Di Paolo, David Ramo Munoz, David Zolst Manrique, Duncan Gowland, Gabriel Greene-Diniz, Georgia Christopoulou, Iakov Polyak, Irfan Khan, Josh Kirsopp, Kentaro Yamamoto, Maria Tudorovskaya, Michal Krompiec, and Nathan Fitzpatrick. Introduction to the inquanto computational chemistry platform for quantum computers, 2022. URL <https://medium.com/cambridge-quantum-computing/4fced08d66cc>.
- [32] Computational chemistry: Inquanto, 2022. URL <https://www.quantinuum.com/products/inquanto>.
- [33] Qiming Sun, Timothy C. Berkelbach, Nick S. Blunt, George H. Booth, Sheng Guo, Zhendong Li, Junzi Liu, James D. McClain, Elvira R. Sayfutyarova, Sandeep Sharma, Sebastian Wouters, and Garnet Kin-Lic Chan. Pyscf: the python-based simulations of chemistry framework. *WIREs Computational Molecular Science*, 8(1):e1340, 2018. doi: <https://doi.org/10.1002/wcms.1340>. URL <https://onlinelibrary.wiley.com/doi/abs/10.1002/wcms.1340>.
- [34] Michael F. Herbst, Maximilian Scheurer, Thomas Fransson, Dirk R. Rehn, and Andreas Dreuw. adcc: A versatile toolkit for rapid development of algebraic-diagrammatic construction methods. *WIREs Computational Molecular Science*, 10(6):e1462, 2020. doi: <https://doi.org/10.1002/wcms.1462>. URL <https://wires.onlinelibrary.wiley.com/doi/abs/10.1002/wcms.1462>.
- [35] J. M. Pino, J. M. Dreiling, C. Figgatt, J. P. Gaebler, S. A. Moses, M. S. Allman, C. H. Baldwin, M. Foss-Feig, D. Hayes, K. Mayer, and et al. Demonstration of the trapped-ion quantum ccd computer architecture. *Nature*, 592(7853):209–213, Apr 2021. ISSN 1476-4687. doi: 10.1038/s41586-021-03318-4. URL <http://dx.doi.org/10.1038/s41586-021-03318-4>.
- [36] Quantinuum h1, powered by honeywell, 2022. URL <https://www.quantinuum.com/products/h1>.
- [37] Seyon Sivarajah, Silas Dilkes, Alexander Cowtan, Will Simmons, Alec Edgington, and Ross Duncan. t|ket>: a retargetable compiler for NISQ devices. *Quantum Science and Technology*, 6(1):014003, nov 2020. doi: 10.1088/2058-9565/ab8e92. URL <https://doi.org/10.1088/2058-9565/ab8e92>.
- [38] Work across platforms with tket, 2022. URL <https://www.quantinuum.com/developers/tket>.
- [39] V.K. Shen, D.W. Siderius, W.P. Krekelberg, and H.W. Hatch. *NIST Standard Reference Simulation Website*. NIST Standard Reference Database Number 173, National Institute of Standards and Technology, Gaithersburg MD, 20899, 2021. doi: <http://doi.org/10.18434/T4M88Q>.
- [40] Joaquin Espinosa-Garcia and Jose C. Corchado. Qct dynamics study of the reaction of hydroxyl radical and methane using a new ab initio fitted full-dimensional analytical potential energy surface. *Theoretical Chemistry Accounts*, 134, 01 2015. doi: 10.1007/s00214-014-1607-1.
- [41] Markus Reiher, Nathan Wiebe, Krysta M. Svore, Dave Wecker, and Matthias Troyer. Elucidating reaction mechanisms on quantum computers. *Proceedings of the National Academy of Sciences*, 114(29):7555–7560, jul 2017. doi: 10.1073/pnas.1619152114. URL <https://doi.org/10.1073/pnas.1619152114>.
- [42] Mario Motta, Gavin O. Jones, Julia E. Rice, Tanvi P. Gujarati, Rei Sakuma, Ieva Liepuoniute, Jeannette M. Garcia, and Yu-ya Ohnishi. Quantum chemistry simulation

- of ground- and excited-state properties of the sulfonium cation on a superconducting quantum processor, 2022. URL <https://arxiv.org/abs/2208.02414>.
- [43] V. E. Elfving, B. W. Broer, M. Webber, J. Gavartin, M. D. Halls, K. P. Lorton, and A. Bochevarov. How will quantum computers provide an industrially relevant computational advantage in quantum chemistry?, 2020. URL <https://arxiv.org/abs/2009.12472>.
- [44] Andrew Zhao, Nicholas C. Rubin, and Akimasa Miyake. Fermionic partial tomography via classical shadows. *Physical Review Letters*, 127(11), sep 2021. doi: 10.1103/physrevlett.127.110504. URL <https://doi.org/10.1103%2Fphysrevlett.127.110504>.
- [45] Seonghoon Choi, Ignacio Loaiza, and Artur F. Izmaylov. Fluid fermionic fragments for optimizing quantum measurements of electronic hamiltonians in the variational quantum eigensolver, 2022. URL <https://arxiv.org/abs/2208.14490>.
- [46] A. Aspuru-Guzik. Simulated quantum computation of molecular energies. *Science*, 309(5741):1704–1707, Sep 2005. ISSN 1095-9203. doi: 10.1126/science.1113479. URL <http://dx.doi.org/10.1126/science.1113479>.
- [47] James D. Whitfield, Jacob Biamonte, and Alán Aspuru-Guzik. Simulation of electronic structure hamiltonians using quantum computers. *Molecular Physics*, 109(5):735–750, Mar 2011. ISSN 1362-3028. doi: 10.1080/00268976.2011.552441. URL <http://dx.doi.org/10.1080/00268976.2011.552441>.
- [48] Jonathan Romero, Ryan Babbush, Jarrod R. McClean, Cornelius Hempel, Peter Love, and Alán Aspuru-Guzik. Strategies for quantum computing molecular energies using the unitary coupled cluster ansatz, 2018.

A UCC Synthesis Methods

UCCSD State-Preparation Methods

The wavefunction describing each molecular system is prepared via a parameterised quantum circuit or ansatz that provides an appropriate description of electron correlation. We use the UCCSD operator. It is represented as a Trotterized product of exponents [25], and mapped to Pauli representation using Jordan–Wigner encoding (JWE) [24, 46]. With JWE, each qubit represents the electron number occupation of each spin-orbital in our system - $|1\rangle$ is occupied and $|0\rangle$ is unoccupied. We use alpha-beta (ab) ordering, so that spatial orbital index p corresponds to even-indexed and odd-indexed spin-orbitals, $2p$ and $2p + 1$. Using JWE leads to a sequence of Pauli- Z operations, necessary to preserve antisymmetry of our UCC state, but at the cost of increasing effective k -locality. We refer to these Pauli- Z operations as JWE-strings.

The UCCSD operator is Trotterized and written as a product of Pauli exponentials via JWE:

$$e^{\hat{T}-\hat{T}^\dagger} \approx \prod_m \prod_n e^{i\theta_m \hat{P}_{m,n}}, \quad (7)$$

where the index m runs over each distinct Fermionic excitation, and index n runs over each Pauli-sub-term, $\hat{P}_{m,n}$, of that Fermionic excitation. In Eq. 7, θ_m are independent real parameters, and \hat{T}^\dagger is the sum over each excitation operator acting across all orbitals. The excitations that are included in the ansatz are determined by the spin-multiplicity, number of electrons and the basis-set size of the chemical system. UCCSD can be very costly in the number of two-qubit gates which has limited its practicality in hardware experiments.

The chemically aware UCC synthesis is described in the methods section. A summary is provided below:

- A symmetry filtering step to discard redundant Fermionic excitations [26].
- A compact synthesis of Fermionic spatial-to-spatial excitations by treating them as Bosonic operations and applying Jordan-Wigner encoding [14]. For each spatial-to-spatial excitation, the two-qubit gate count is reduced from 64 to 2 [12].
- A Pauli-Gadget synthesis method leveraging commuting property of observables, available in tket [21]. This is used to synthesise generic double UCC excitations and single UCC excitations.

We compare the chemically aware state-preparation with commuting sets and individual synthesis in Sec. 2.1. A description for the latter two methods is provided below.

Commuting Sets

A UCC synthesis method leveraging commuting property of observables, available in tket, [21]. The full set of single and double UCC excitations are generated for a specific Fermionic reference state, no additional filtering based on symmetry or any other chemical analysis is performed. The default ordering of the UCC excitations is not changed, i.e. singles are synthesised before doubles. Within our study, we use each UCC excitation as its own distinct commuting set. UCC double excitations with length zero JWE-strings can be synthesised with 14 two-qubit gates. Excitations with arbitrary length JWE-strings have a two-qubit count greater than 14.

The Pauli-sub-terms within the ansatz can be intermixed to achieve more favourable two-qubit gate cancellation (caused by JW-strings), but this is not performed here. We are not sure how this would affect Trotter error.

Individual

Brute-force synthesis of UCC excitations. Each Pauli-sub-term for each Fermionic excitation is synthesised with the Hadamard gate, \hat{R}_x with fixed gate rotation $\pm\pi/4$, a cascade of two-qubit gates and a arbitrary phase $\hat{R}_z(\theta)$ rotation gate. A circuit primitive for $e^{-\pi/2\theta\hat{Y}_0\hat{X}_1\hat{Z}_2}$ is shown in Fig. 4. Ref. [47] and Ref. [48] provide more details on this.

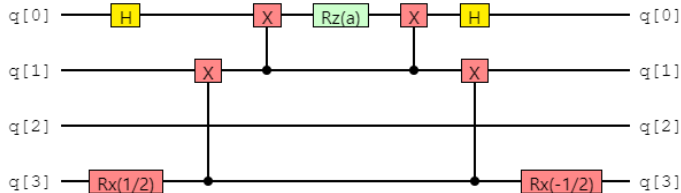


Fig. 4. A circuit primitive for $e^{-\pi/2\theta\hat{P}}$, where \hat{P} is $\hat{Y}_0\hat{X}_1\hat{Z}_2$. Circuit is visualised with tket.

B CH₄ 6-qubit active space model

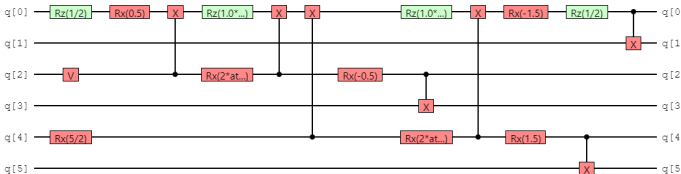


Fig. 5. Chemically aware UCC circuit containing only two spatial to spatial orbital double excitations. The other double and single excitations are discarded as part of the chemically aware procedure.

InQuanto-PySCF describes MOs of CH₄ with the point group D_2 . In the active-space, the occupied orbital has irrep b_3 , and two degenerate virtual orbitals have irrep b_1 and b_2 . There are two U_1 symmetry operators corresponding to alpha- and beta-electron number conservation. There are two further operations corresponding to π radian rotations of the CH₄ molecule around z - and y -axes:

- $\hat{C}_z(\pi/2) : \hat{Z}_0\hat{Z}_1\hat{Z}_2\hat{Z}_3;$
- $\hat{C}_y(\pi/2) : \hat{Z}_0\hat{Z}_1\hat{Z}_4\hat{Z}_5.$

We employ these symmetries in the chemically aware strategy resulting in only two spatial to spatial doubles (two-qubit gate count 7). The circuit used for CH₄ calculations is shown in Fig. 5.

For the calculations in this paper, we built chemical models with InQuanto-PySCF for the following reaction participants, CH₄, CH₃, H₂O, OH \cdot , and [CH₃ - H - OH] \ddagger . We used minimal basis

and neutral electrostatic charge for all species. For the closed-shell (open-shell) species we used an active space of three spatial orbitals and two (three) electrons. CASSCF was used to optimize for the active space of choice. For certain species, the guess point group assigned by PySCF affected the amount of correlation recoverable with UCC-VQE or Post-HF methods (CCSD). In Tab. 3, we report electronic correlation energy for CH₄ when using C₁ or D₂ point groups with (CASSCF orbitals) and without (SCF orbitals) orbital optimization.

Table 3. Table showing correlation energy (Ha) in CH₄ when using CASSCF and SCF orbitals with D₂ or C₁ point group symmetry.

Point Group	CASSCF Orbitals	SCF Orbitals
D ₂	-0.0026	-0.0026
C ₁	-0.0158	-0.0105

C Trotter Error in CH₃ 6-qubit Chemically Aware UCC Circuit

For CH₃ after parametric compilation, we note an initial decrease from 88 two-qubit gates to 50 two-qubit gates for the chemically aware circuit. This is due to the excitation reordering step which also changes the optimal parameters for those excitations. To achieve the two-qubit gate count of 20 for CH₃ with chemically aware, we defined an absolute tolerance (1×10^{-4}) to discard small excitations ($\hat{a}_4^\dagger \hat{a}_2 \hat{a}_3^\dagger \hat{a}_1 - h.c.$). We report the subset of excitations synthesised on the chemically aware and commuting sets circuit in Tab. 4.

Table 4. Showing CH₃ UCC excitations with their ordering and optimal parameters on chemically aware[†] and commuting sets[⊥] circuit. Optimal parameters defined as UCC angles in radians.

Exponents	Order [†]	Order [⊥]	Angle [†]	Angle [⊥]
$\hat{a}_4^\dagger \hat{a}_0 \hat{a}_5^\dagger \hat{a}_1 - h.c.$	1	6	-0.03611	-0.07243
$\hat{a}_4^\dagger \hat{a}_2 \hat{a}_3^\dagger \hat{a}_1 - h.c.$	2	7	-0.00009	0
$\hat{a}_4^\dagger \hat{a}_0 - h.c.$	3	0	0.00117	0
$\hat{a}_5^\dagger \hat{a}_1 - h.c.$	4	1	0.00132	0

D Symmetry Verification

Partition Measurement Symmetry Verification

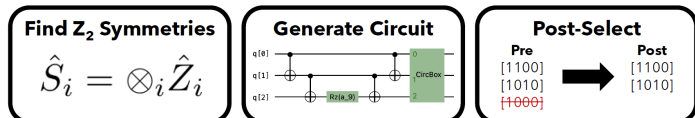


Fig. 6. Schematic detailing pre- and post-processing steps to execute Partition Measurement Symmetry Verification.

The aim of PMSV (Partition Measurement Symmetry Verification) is to apply a constraint to the measurement result of

some quantum computation that can be used in classical post-processing to improve upon the quality of calculation. Certain physical symmetries can be represented as Pauli-symmetries by keeping track of parity. In this paper, we exploit Z_2 symmetries such as mirror planes or unit cell translations and U_1 symmetries such as electron number conservation [27, 26, 17]. If applicable to the problem, PMSV can be performed without increasing the number of measurement circuits. There is a small resource increase to measure the additional Pauli-symmetries, either extra two-qubit gates as part of the diagonalization process in measurement reduction, or measuring more qubits for a particular measurement circuit. We state the recipe for PMSV here:

- (1) Find largest Abelian point group of molecule. Transformations of this point group are Pauli-symmetries.
- (2) Build symmetry verifiable circuits using the measurement reduction facility in tket. The operators that we need to measure on the quantum device to solve out problem consist of Pauli-Is, Pauli-Xs, Pauli-Ys and Pauli-Zs across the qubit register. These operations can be partitioned into commuting sets. For element in a commuting set, if the Pauli-symmetries commute element-wise, it can be added to the commuting set. This way, each commuting set is symmetry verifiable.
- (3) Post-select on measurement result before counting bit-strings to compute expectation value of problem Hamiltonian. The quantity to post-select on is the XOR sum over the bit-strings needed to compute expectation value of Pauli-symmetry.

Mid-circuit Measurement Symmetry Verification

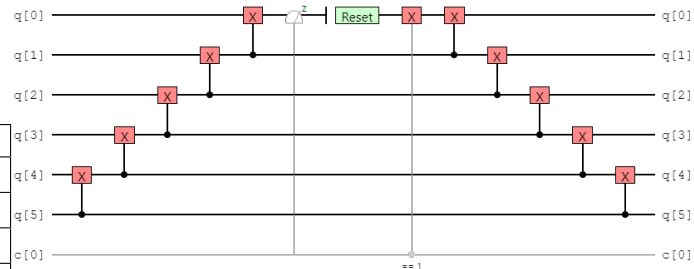


Fig. 7. Circuit primitive to project into the -1 sector of the Pauli Symmetry $\hat{Z}_0 \hat{Z}_1 \hat{Z}_2 \hat{Z}_3 \hat{Z}_4 \hat{Z}_5$.

Mid-measurement symmetry-verification checks if a symmetry has been violated during runtime of the quantum circuit, and discards measurement results based on this check [23]. This technique has a 2-qubit gate penalty. For this problem, mid-circuit measurements were used to enforce total electron number conservation: adding 10 two-qubit gates to the measurement circuits.

Measuring the qubit in the middle leaves the qubit in a non-computational basis. Hence, we reset the qubit to the state, $|0\rangle$, followed by a classically conditioned reset on the classical bit, $c[0]$, to allow further simulation of the quantum circuit. To perform the projection,

$$\hat{P} = \hat{I} + (-1)^x \hat{S} \quad (8)$$

normally one requires measuring each qubit. \hat{S} is the Pauli-Symmetry and x is the parity of the bitstring to accept or reject. We can transfer this measurement to only one qubit by using a CX gate cascade. The circuit primitive we use to project the state

into a particular symmetry sector is given in Fig. 7. We note that to symmetry verify each measurement circuit, the conflicting sets of Pauli-strings need to be synthesized into measurement circuit, hence introducing additional two-qubit gate. For the systems studied, the additional number of two-qubit gates is very small.

E Data from Experiments

Electronic ground state energy of CH₄ computed H1-2

Data from the H1-2 ground-state calculation in Sec. 2.1. Jensen-Shannon Divergence of the measured distributions corresponding to the simulated circuits are also displayed in Fig. 2

Table 5. Electronic Energy of CH₄ with 6-qubit active space and chemically aware state-preparation circuit computed on H1-2.

	Energy (Ha)	Rel. Error (%)
Raw	-39.656	0.184
PMSV₁	-39.695	0.086
PMSV₂	-39.721	0.020

Ground state energies of the refrigerant molecules

Data behind the reaction barrier calculation in Sec. 2.3, Tab. 2.

Table 6. Results from Hamiltonian averaging experiments on H1 and H1E. All molecules are simulated on H1-1, except for CH₄ which is simulated on H1-2. Parameters characterizing ground-state are found via a noiseless VQE execution on *qasm* simulator. Noiseless energy from *qasm* is also displayed as a benchmark.

Molecule	H1-1E (Ha)	H1 (Ha)	qasm (Ha)
OH	-74.34	-74.29	-74.36
H ₂ O	-74.92	-74.77	-74.97
CH ₃	-39.05	-38.94	-39.08
CH ₄	-39.72	-39.72	-39.73
[CH ₃ -H-OH] [‡]	-113.98	-113.77	-114.04